Environmental Pollution 241 (2018) 912–921

Contents lists available at ScienceDirect

Environmental Pollution

journal homepage: www.elsevier.com/locate/envpol

Colloidal stability of Fe_3O_4 magnetic nanoparticles differentially impacted by dissolved organic matter and cations in synthetic and naturally-occurred environmental waters☆

Hao Wang [a, b], Xiaoli Zhao [a, *], Xuejiao Han [a], Zhi Tang [a], Fanhao Song [a], Shaoyang Zhang [c], Yuanrong Zhu [a], Wenjing Guo [a], Zhongqi He [d], Qingwei Guo [b], Fengchang Wu [a], Xiaoguang Meng [e], John P. Giesy [a, f]

[a] State Key Laboratory of Environmental Criteria and Risk Assessment, Chinese Research Academy of Environmental Sciences, Beijing 100012, China
[b] South China Institute of Environmental Sciences, Ministry of Environmental Protection, Guangzhou, China
[c] College of Geoscience and Surveying Engineering, China University Mining and Technology, Beijing 100083, China
[d] USDA-ARS Southern Regional Research Center, 1100 Robert E Lee Blvd, New Orleans, LA 70124, USA
[e] Center for Environmental Systems, Stevens Institute of Technology, Hoboken, NJ 07030, USA
[f] Department of Biomedical and Veterinary Biosciences and Toxicology Centre, University of Saskatchewan, Saskatoon, Saskatchewan, Canada

ARTICLE INFO

Article history:
Received 23 March 2018
Received in revised form
16 May 2018
Accepted 9 June 2018
Available online 14 June 2018

Keywords:
Suspension and aggregation
Magnetic nanoparticles
Humic acid
Fulvic acid
Metal cations
Environmental waters

ABSTRACT

Better understanding of the colloidal behaviors of nanomaterials impacted by aquatic chemistry parameters is needed for appropriate evaluation of the environmental risks posed by nanomaterials in natural waters. In the study, the colloidal stability of Fe_3O_4 magnetic nanoparticles (Fe-MNPs) was evaluated over a range of chemistry characteristics [e.g., pH, dissolved organic matter (DOM), salt types, cationic strength] in six synthetic water samples. The findings from the synthetic water samples were further examined with eight "real world" environmental water samples. Our results demonstrated that DOM fraction, humic acid (HA), promoted suspension of Fe-MNPs more by hydrophobic interactions in addition to ligand exchange and electrostatic effects compared with fulvic acid (FA). Capability of cations to increase aggregation of Fe-MNPs were in the order of $Ca^{2+} > Mg^{2+} >> Na^{+}$ because of their different degrees of bridging complexation with DOM molecules on particle surfaces. As a key parameter for indicating Fe-MNPs colloidal stability, Zeta (ζ) potentials of Fe-MNPs in these waters samples were well correlated to ($R^2 = 0.880$, $P < 0.001$) the contents, types and adsorption forms of DOM and cations. However, several other factors could also affect the hydrodynamic diameter (HDD) of Fe-MNPs in the "real world" environmental waters. It assumed that ampholytic-DOM molecules such as amino acid- and protein-like molecules caused great aggregation of Fe-MNPs. These findings would be helpful for better understanding and evaluating the colloidal behaviors of nanomaterials when they released into natural water environment, thus could shed light on developing relevant pollution control strategies.

1. Introduction

Nanomaterials (NMs) are nano-objects having a size range of 1–100 nm, at least in one dimension (Amde et al., 2017). In the past decades, NMs have shown their widespread applications in many fields such as industries, agriculture and environment (Guo et al., 2016; Luna-Valdez et al., 2017; Taghiyari et al., 2017; Yang and Xing, 2009). On the other hand, the rapid increase of NMs products and applications open the door for their intentional and unintentional release to the environment, leading to the serious environmental concern (Gottschalk et al., 2013; Lei et al., 2018; Zhu et al., 2017). For example, while the superparamagnetism of Fe_3O_4 magnetic nanoparticles (Fe-MNPs) facilitates their applications as a carrier in biomedicine, pharmaceutical, detection for trace

☆ This paper has been recommended for acceptance by Baoshan Xing.
* Corresponding author.
E-mail address: zhaoxiaoli_zxl@126.com (X. Zhao).

https://doi.org/10.1016/j.envpol.2018.06.029
0269-7491/

pollution and water purification (Reddy et al., 2012; Rossi et al., 2014), the same unique property makes Fe-MNPs highly dynamic in aquatic environment, which could affect its colloidal stability, transport and transformation, so does on its fate and toxicity (Amde et al., 2017; Lei et al., 2018; Zhu et al., 2017).

In aqueous ecosystems, suspension and aggregation of nanomaterials are the key factors in determining their hazards and risks as suspended (i.e., colloidal) particles have a higher mobility due to the effects of hydrodynamic forces and a high risk to organisms due to more active reaction sites exposed to the surface compared to particles that are aggregated (Godinez and Darnault, 2011; Jian Zhao et al., 2013). Nanomaterials could interact with numerous components of environmental waters with dissolved organic matter (DOM) and inorganic ions as the two major components (Aiken et al., 2011; Philippe and Schaumann, 2014; Wiesner et al., 2006). DOM including humic acid (HA) and fulvic acid (FA) can coat the surfaces of nanomaterials unselectively by ligand exchange, electrostatic, H-bonding and hydrophobic interactions, which facilitates suspension and bioaccumulation of nanomaterials (Johnson et al., 2009; Saleh et al., 2008; Vindedahl et al., 2016). In contrast, metal cations cause aggregation of nanoparticles by neutralizing negative charges after adsorbing on the surface of nanomaterials (Aiken et al., 2011; Bian et al., 2011).

Environmental behaviors and physicochemical properties of nanomaterials are generally determined by specific interaction types of water components with nanomaterials. Improved understanding on these interactions are needed for evaluating more actually colloidal behaviors of nanomaterials in natural waters (Philippe and Schaumann, 2014). In addition to FA, HA and inorganic ions, thousands of other components are also present in environmental waters, such as carbohydrates, amino acids, proteins, organic acids, surfactants (Amarasiriwardena et al., 2001; He et al., 2013; Liu et al., 2018; Ohno et al., 2010). Moreover, the classical colloid theories [e.g., classical Derjaguin-Landau-Verwey-Overbeek (DLVO) model] have significant limitations in assessing the colloidal behavior of engineered nanoparticles in natural waters (Ghosh et al., 2011; Ghosh et al., 2008; Ghosh et al., 2014). These complicities make it fail to predict the stability of colloids in environmental waters although DLVO model has been applied to quantify the effects of inorganic ions on the stability of nanomaterials. Therefore, it seems necessary to identify more specifically the primary factors and related interactions affecting the aggregation and suspension of nanomaterials in waters. To our knowledge, the stability of nanomaterial has not been investigated systematically for a range of environmental conditions so far.

As one of the most important magnetic nanoparticles, most, if not all, Fe-MNPs are released into the environment during the processes of production, transportation, application and disposal and eventually enter into aquatic ecosystems. Nevertheless, there is only limited information available on colloidal stability of Fe-MNPs affected by aquatic chemistry parameters (Dong et al., 2016; Ghosh et al., 2011; Lei et al., 2018). In this study, we hypothesized that DOM and cations, but with different impact modes and levels were two major factors in the influence of the colloidal stability of Fe-MNPs. To verify the hypothesis, we first examined the several colloidal stability parameters impacted quantitatively by representative DOM fractions (HA and FA), and common mono- and divalent cations (Na^+, Mg^{2+} and Ca^{2+}) in six synthetic water samples under laboratory conditions. Dynamics modelling and advanced spectroscopic techniques were applied to understand the impact mechanisms. Then, we examined the aggregation behaviors of Fe-MNPs in eight naturally-occurred environmental waters (river/lake waters, tap water, sea water, rain water, domestic sewage), and yielded data were further used to develop predictive colloidal behaviors of Fe-MNPs in “real world” environmental waters.

2. Materials and methods

2.1. Materials

All chemical reagents used in the study were of analytical purity. FA (No. 1R105F) from Nordic reservoir and HA (No. 2S101H) from Suwannee River were purchased from the International Humic Substances Society (IHSS, Colorado, USA). The two humic fractions used in this research were representatives of aquatic dissolved organic matter that contain multiple soluble organic components (He et al., 2006; He et al., 2008). Water (18.2 MΩ cm) was supplied by a Millipore Integral 5 water purification system (Merck, Germany). Fe-MNPs were synthesized by co-precipitation (Xiaoli Zhao et al., 2008). Characteristics of Fe-MNPs have been reported in our previous work (Wang et al., 2015). Oxygen-free water was used to wash repeatedly the Fe-MNPs sample to remove inorganic ions with the concentration of Na^+ less than 0.5 mM (detected with a DX223-Na sodium electrode) (Mettler Toledo, Switzerland).

2.2. Water samples

Synthetic waters (S1, S2, S3, S4, S5 and S6) were prepared with Na^+, Mg^{2+}, Ca^{2+} and FA, and additional details are described in the Supporting Information (SI). Eight “real world” water samples were collected for this study. Tap water (TW) was collected from the faucet of the laboratory itself (Beijing, China); urban river water from Qing River (QHW, Beijing, China); fresh lake water from Dianchi Lake (DCW, Kunming, China). Rainwater (RW) was collected during July 2016 (Chaoyang, Beijing). Two relatively uncontaminated natural water samples were collected from Muyun Reservoir (MYW, Beijing, China) and Dari River (DRW, Tibet, China). Domestic sewage (DSW) was sampled from a stagnant pool on the Sha River (Beijing, China); and a seawater (SW) sample was collected from offshore of Qingdao (China). All samples were stored at 4 °C after filtration through 0.45-μm polyethersulfone filters.

2.3. Laboratory batch experiments with synthetic waters

Adsorption kinetics of FA and HA (10.0 mg/L) on Fe-MNPs (50 mg/L) were determined. First, pHs of the experimental mixtures were adjusted to 5.0, 7.0 and 9.0 with KOH (1.0 mM) and HCl (1.0 mM), respectively. Then, suspensions were shaken at 100 r/min, and sampled at intervals from 0.5 to 72 h. Total organic carbon (TOC) of the supernatant of each mixture was measured after filtration through a 0.2-μm polyethersulfone membrane (Pall Corporation, Michigan).

For investigating aggregation of Fe-MNPs, Fe-MNPs was added into FA or HA solution (40 mL), respectively. pH of each sample was maintained at 5.0, 7.0 or 9.0. After sonification for 0.5 min, zeta (ζ) potential and hydrodynamic diameter (HDD) of each mixture were measured by laser Doppler velocimetry (LDV) and dynamic light scattering (DLS). Effects of Na^+ (1.0–100.0 mM), Mg^{2+} and Ca^{2+} (0.1–25.0 mM) on aggregation of Fe-MNPs in the presence of FA or HA (10 mg/L) were evaluated in the same way. Fe-MNPs were collected by a magnetic field and freeze-drying. Supernatants were also collected for quantification of free metal cations and HA/FA after filtration.

ζ potential and HDD of Fe-MNPs were measured by a Zetasizer Nano meter (Malvern, England). TOC was quantified by a Multi N/C3100 TOC analyzer (Analytikjena, Germany). Concentrations of metal cations were measured by an inductively coupled plasma-optical emission spectrometer (ICP-OES, iCAP 6300, Thermo Scientific, Massachusetts, USA). Bonding features and abundance of FA, HA and metal cations adsorbed on Fe-MNPs were investigated by FTIR spectrometer (Nicolet iS5, Thermo Scientific,

Massachusetts, USA) and X-ray absorption near edge structure (XANES). The number of FTIR scans and corresponding wavenumber resolution were 32 times and 0.5 cm^{-1} respectively, and KBr pallet was made to record FTIR spectra. K-edge spectra of Ca-adsorbed Fe-MNPs were collected at beam-line 9M-B, C at the Advanced Photo Sources (APS), Argonne National Laboratory (Illinois, USA). An energy range of −200 to 200 eV from the K-edge was used to acquire the spectra with a passivated implanted planar silicon (PIPS) detector. Three scans were collected from each sample, inspected for overall quality, and averaged to improve the signal/noise ratio. The XANES data was normalized using the ATHENA program in the Demeter computer package (Newville, 2001; Ravel and Newville, 2005). Superconducting Quantum Interference Device (SQUID, Quantum Design, USA) was used to analyze the effect of DOM on magnetic properties of Fe-MNPs. All data statistical analysis in the study was finished with Origin Pro 8.0.

2.4. Adsorption isotherm modelling

Adsorptions of FA and HA on Fe-MNPs were described with Langmuir and Freundlich isotherm models (1 and 2).

$$q_e = \frac{q_m K_L C_e}{1 + K_L C_e} \leftrightarrow \frac{C_e}{q_e} = \frac{1}{q_m K_L} + \frac{C_e}{q_m} \quad (1)$$

$$q_e = K_F C_e^{1/n} \leftrightarrow lgq_e = lgK_F + \frac{1}{n} lgC_e \quad (2)$$

Where: q_e is the adsorbed amount of FA or HA per gram of Fe-MNPs at equilibrium adsorption; q_m and C_e are the maximum adsorption and equilibrium concentrations of FA or HA; K_L and K_F are the adsorption equilibrium constants of Langmuir and Freundlich models respectively; n is another Freundlich constant indicating the intensity of adsorption.

2.5. Colloidal behaviors of Fe-MNPs in environmental waters

Fluorescence spectra of environmental water samples were measured with a Hitach F-7000 spectrophotometer (Tokyo, Japan) at room temperature. The operating voltage was 600 V, and slit widths were 5.0 nm for excitation (Ex) and emission (Em) (He et al., 2008). Of each sample, ζ potential and HDD of Fe-MNPs (50 mg/L), as well as TOC and cationic concentrations were measured before and after adsorption respectively.

3. Results and discussion

3.1. Effects of HA and FA on suspension and aggregation of Fe-MNPs in synthetic waters

FA and HA were observed to greatly promote the suspension degree of Fe-MNPs due to their negative charges increased on the particle surface, especially with the conditions at pH 7.0 and 9.0. HA presented greater ability for strengthening ζ potential and suspension of Fe-MNPs than FA (Fig. 1a–b). The difference might be related to their specific adsorption mechanisms of FA and HA on Fe-MNPs. As shown in their kinetic and isotherms adsorptions, the amounts of HA adsorbed on the particles were higher than those of corresponding FA with all pH conditions (Fig. S1). Adsorption isotherms for binding of FA and HA on Fe-MNPs were further fitted with Langmuir and Freundlich models. Results showed that adsorption of FA on Fe-MNPs at all pHs were better fitted by the Langmuir model (Fig. 1c and Table S1). This observation indicates that monolayer adsorption of FA was formed on Fe-MNPs. Ligand exchange might be responsible for FA adsorption due to relatively high binding affinity of iron ion with carboxyl group, and the same results were observed by Filius (Filius et al., 2000; Filius et al., 2003). On the other hand, adsorptions of HA was fitted better to Langmuir model for pH 7.0 and 9.0, but 5.0 where Freundlich model was more suitable. The differential observations with HA data suggest that multilayer adsorption of HA might be developed at pH 5.0, but monolayer adsorption was formed under higher pH conditions. The possible mechanism would be that HA presented great hydrophobicity at acidic conditions, which mainly promoted multilayer adsorption of HA on the particles besides ligand exchange interaction. However, with the increase of deprotonation of HA molecules at higher pH, the hydrophobicity capability gradually decreased, the adsorption of HA tended towards monolayer formation (refer to SI for more discussion).

As FA and HA are organic matter with multiple functional structures (He et al., 2013; He et al., 2010; Ohno et al., 2010), so that they could not be regarded as simple inorganic ions in evaluating their effects on the colloidal stability of Fe-MNPs by traditional colloid theory. In this work, we observed that the stability of Fe-MNPs was greatly dependent on the ζ potential of Fe-MNPs. Furthermore, the negative charges increased gradually as a function of increasing concentrations of FA or HA. We also observed excellent linear relationships ($R^2 > 0.99$) between the concentration of FA or HA and ratios of the concentrations/ζ potentials of Fe-MNPs (Fig. 1d). In other words, the ζ potential of Fe-MNPs was mainly influenced by the specific adsorption characteristics of FA and HA on the particles. This finding shed novel light in evaluating the stability of Fe-MNPs.

3.2. Effects of metal cations on suspension and aggregation of Fe-MNPs in synthetic waters in the presence of HA or FA

Jointly with HA or FA, the ions of Na^+, Mg^{2+} and Ca^{2+} as major constituents of natural water generally influence stability behaviors of Fe-MNPs. Per our previous study, adsorption of these cations on Fe-MNPs could largely increase positive charges of the particle surface via the effects of hydration and electrostatic forces, and eventually affected colloidal stability of Fe-MNPs (Wang et al., 2017). In this study, the negative ζ potential of Fe-MNPs was neutralized gradually with the addition of the metal cations resulting in the decrease of electrostatic repulsion between Fe-MNPs so that the Fe-MNPs aggregation occurred (Fig. 2). The capability of the cations in neutralizing ζ potential and increasing the HDD of Fe-MNPs were observed in the order: $Ca^{2+} > Mg^{2+} > Na^+$. Simultaneously, the amounts of the cations adsorbed on the particles also increased greatly with their concentrations (Fig. S3c-d). Therefore, ζ potential of Fe-MNPs could be regulated by the adsorbed metal cations. Moreover, the cations remarkably promoted the adsorptions of FA and HA on Fe-MNPs, of which the capability could be also ranked as $Ca^{2+} > Mg^{2+} >> Na^+$ (Fig. S3a-b). These observations indicate that multilayer adsorption of organic molecules and metal cations tended to happen on the surface of Fe-MNPs via the effect of electrostatic interactions. Fitted in Freundlich isotherm model, significant ($P \leq 0.05$) linear relationships were observed between the ζ potential of Fe-MNPs and the logarithmic concentrations of the metal cations (Fig. 3). These observations were similar to the colloidal behaviors of HA- and synthetic poly (acrylic acid)-coated ferrimagnetic (γFe_2O_3) nanoparticles (Ghosh et al., 2011) and partially similar to that influence of FA on the colloidal stability of zero-valent iron nanoparticles (Dong et al., 2016).

In this study, divalent Ca^{2+} or Mg^{2+} changed the ζ potential and HDD of Fe-MNPs more than did by monovalent Na^+ at the same or relatively less ionic strength (Fig. 2a–b). As this observation cannot

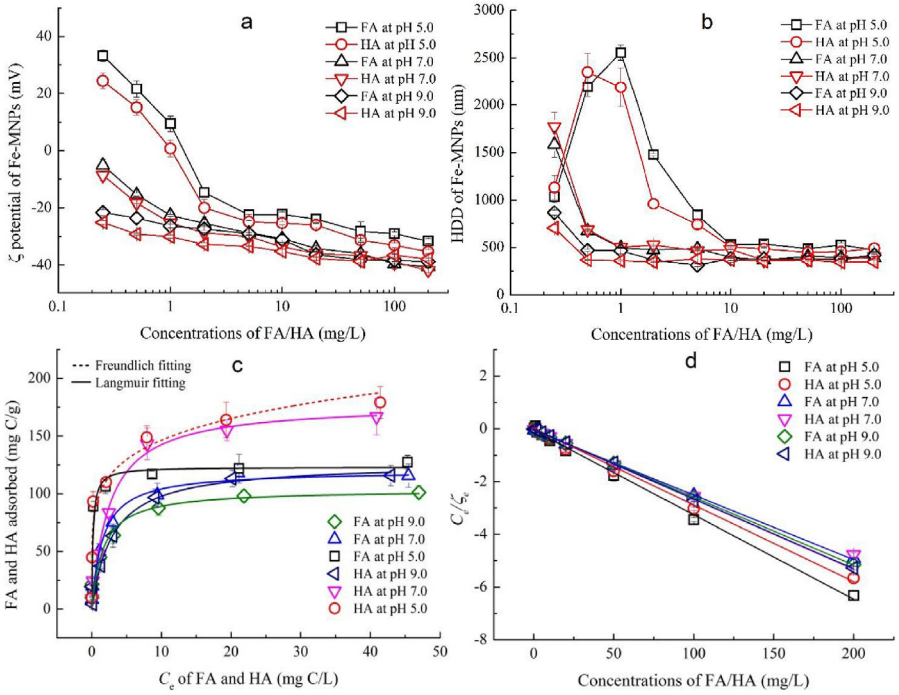

Fig. 1. ζ potential (a) and HDD (b) of Fe-MNPs, isothermal adsorption of DOM (c) and linear fittings of ζ potential of Fe-MNPS (d) as functions of FA and HA at pH 5.0, 7.0 and 9.0.

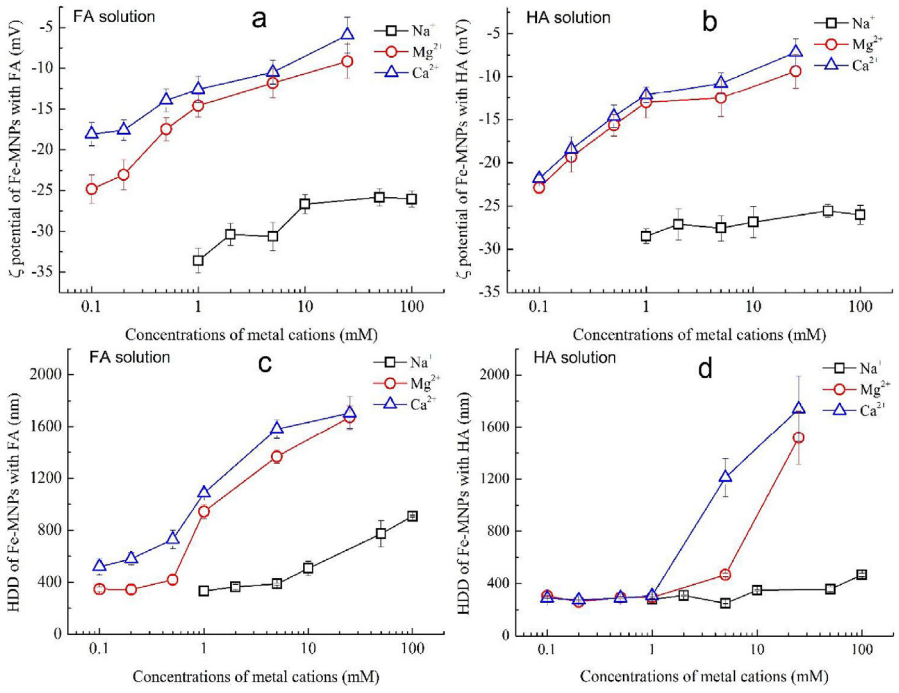

Fig. 2. Effects of Na^+, Mg^{2+} and Ca^{2+} on ζ potential (a, b) and HDD (c, d) of Fe-MNPs in FA and HA (10.0 mg/L) solutions respectively.

be explained by traditional colloid theory (Boström et al., 2001), we hypothesized that other mechanisms could be involved in the process. It was reported that cations with larger ionic radii can bind to the carboxyl group of particles (e.g., graphene oxide) more intensively by forming inner-sphere complexes (Erhayem and Sohn, 2014; Filius et al., 2000; Xia et al., 2017). Due to its relatively larger ionic radius and higher valence state, Ca^{2+} possessed a greater affinity to FA and HA molecules than Mg^{2+} and Na^+. This assumption appears consistent with the solubility product constants (K_{sp}) of their oxalate salts (2.32×10^{-9} for Ca^{2+} and 4.83×10^{-6} for Mg^{2+}). Based on our previous work, cations with larger ionic radii have a relatively lower affinity to water molecules, and could bond to Fe-MNPs more heavily via the effects of van der Waals forces. Same phenomenon was also observed for graphene oxide (Wang et al., 2017; Xia et al., 2017). Therefore, in addition to electrostatic interaction, some other factors might be involved in

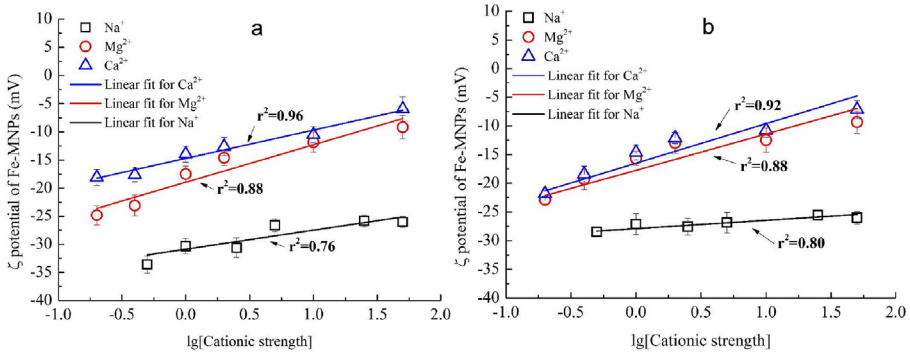

Fig. 3. Linear correlations of the ζ potential of Fe-MNPs with the concentrations of metal cations in FA (a) and HA (b) solutions.

affecting the stability of Fe-MNPs through changing binding types of these cations and DOM molecules on Fe-MNPs, such as cationic hydration, specific ion effects (Kunz, 2010).

3.3. Spectroscopic features of FA and HA on Fe-MNPs affected by Na^+, $Mg^{2+}$and Ca^{2+}

FTIR spectral features of both HA and FA in the absence of cations were typical for the two types of samples (He et al., 2006), so that only the spectral features in the lower-wave-number ranges were presented for clarity (Fig. 4). Greater red-shift of asymmetric stretching vibrations (ν_{as} around 1600 cm^{-1}) of carboxylic groups of adsorbed FA and HA was observed with Mg^{2+} and Ca^{2+} compared with Na^+. Monovalent Na^+ could be the main counter ion while the carboxyl groups of FA and HA are deprotonated as COO^- (Leenheer et al., 1995). Relatively stronger electrostatic affinities of Mg^{2+} and Ca^{2+} to carboxylic groups facilitated their substitution for Na^+ to bind organic molecules, which caused significant red-shift of the ν_{as} of carboxylic groups (Fig. 4). Moreover, due to a relatively lesser hydration capability than Mg^{2+}, Ca^{2+} could more easily overcome the resistance of its surrounding water molecules to bind to carboxylic groups of DOM, and resulted in further decrease of the ν_{as} (Fig. 4c and e) (Wang et al., 2017; Xia et al., 2017). In addition, the initial ν_{as} of carboxylic groups in HA was observed at 1617 cm^{-1}, but 1621 cm^{-1} for FA, and the difference between FA and HA possibly ascribes to their specific pK_a values. The pK_a of HA is generally greater than that of FA and ranges from 2.5 to 9.0, which indicates a larger protonation capability for HA molecules (Abate and Masini, 2001; Paul et al., 2015). At pH 7.0, part of carboxylic groups of HA still protonated, so that the additive metal cations could partly substitute for hydrogen to bind to carboxylic groups. As a result, all of the metal cations caused the red-shift of the carboxylic groups of HA more greatly compared with FA (Fig. 4b, d and f).

For quantitative comparison, the FTIR peak (band) of the carbonyl groups at 1723 cm^{-1} was used as a reference to calibrate impacts of FA and HA on Fe-MNPs. Band intensity of carboxyl group at 1620 cm^{-1} would be an indicator to characterize the HA or FA fractions absorbed to Fe-MNPs particles. Results indicated that adsorptions of FA and HA were enhanced by all three cations, but significant differences in the adsorbed abundance were observed among them (Fig. S4). Specifically, for same I_c, capacities of the three metal cations to increase band intensity of peaks associated with carboxylic groups of FA was: $Na^+ > Mg^{2+} > Ca^{2+}$. Given less adsorption amounts of FA in Na^+ solutions (Fig. S3a), these data suggested that Na^+ preferred promoting adsorption of FA that contained multiple carboxylic groups on Fe-MNPs, and resulted in a significant increase in adsorption intensity of carboxylic groups (Fig. S4a). In contrast, Ca^{2+} and Mg^{2+} exhibited greater affinities for carboxylic groups, even those molecules containing a single carboxyl group, which resulted in relatively less discriminative adsorption of DOM molecules on Fe-MNPs among the cations (Fig. S4c and e). For HA adsorption, an inverse trend for adsorption of HA was observed in the order: $Ca^{2+} > Mg^{2+} > Na^+$ (Fig. S4b, d and f). The probable explanation might be that HA molecules are generally larger size and contain multiple carboxylic groups, which largely decreased discriminative adsorption of different DOM molecules on particles (Erhayem and Sohn, 2014). In addition, the adsorbed Ca^{2+} on Fe-MNPs in the presence of FA was examined by Ca K-edge XANES spectroscopy (Fig. 5). Its characteristic XANES peaks was same to those of $CaCO_3$, indicating that Ca^{2+} was complexed with carboxyl group of FA molecules on the surface of Fe-MNPs. Therefore, combining the results of FTIR and XANES, the capability of Na^+, Mg^{2+} and Ca^{2+} to affect stability of Fe-MNPs was determined by their affinity to DOM molecules by forming complexes (outer- or inner-sphere complexes) with DOM molecules on the particle surface. Consequently, due to differences in valence, hydration capability of metal cations as well as structure and functional groups of DOM molecules, the colloid stability of Fe-MNPs in aquatic environment becomes more complex. Nevertheless, by electrostatic effect as well as bridging complexation, the metal cations promoted multilayer adsorption of DOM on Fe-MNPs more efficiently, and eventually affected the ζ potential and HDD of Fe-MNPs, which might be instructive for evaluating the colloid behavior of Fe-MNPs.

3.4. Colloidal stability of Fe-MNPs in environmental waters

For the “real world” environmental applications, the colloidal stability of Fe-MNPs was then evaluated for 8 environmental waters (seawater, river waters, tap water, rain water and sewage water). Generally, ζ potentials of the particles were proportional to concentrations of DOM in these environmental waters (Fig. 6a). However, the trend was also affected by metal cations. For example, because of a high I_c, the negative ζ potential of Fe-MNPs was largely neutralized for SW (Table 1). In the study, an evaluation model ($R^2 = 0.880$, $P < 0.001$) was developed based on the concentrations of DOM and metal cation of 12 waters samples (Tables 1 and 2). Leave-one-out cross validation method was used to check reliability and accuracy of the model (Wu et al., 2013). Result indicates that the model was quite qualified for evaluating the ζ potential of Fe-MNPs in environmental waters based on all of P values < 0.001, as well as 0.24 (<0.30) for difference value between R^2 and R^2_{CV} (Table S4). DRW and MYW samples were also employed to verify

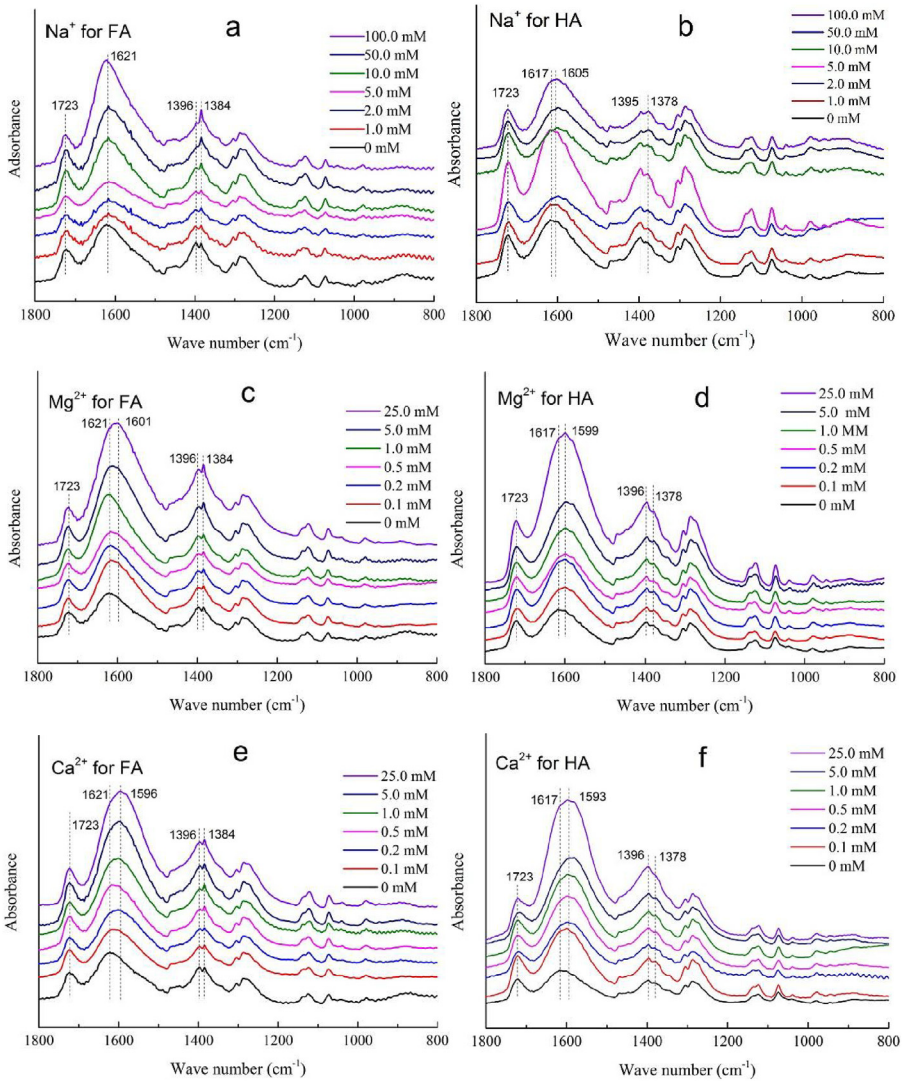

Fig. 4. FTIR spectra of Fe-MNPs coated with HA/FA as functions of metal cations. 10.0 mg/L FA for Na^+ (a), Mg^{2+} (c) and Ca^{2+} (e); 10.0 mg/L HA for Na^+ (b), Mg^{2+} (d) and Ca^{2+} (f).

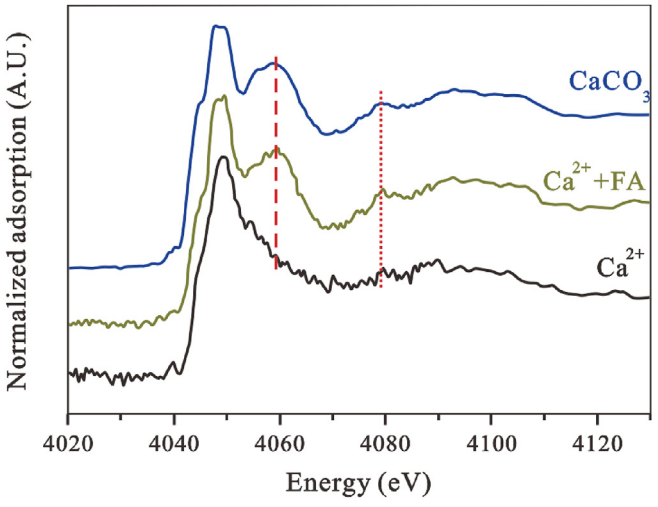

Fig. 5. Ca K-edge XANES spectra of Fe-MNPs. Dashed and dot lines highlight two characteristic peaks.

the model, and results indicated that evaluated ζ potential values of Fe-MNPs for the both natural waters were in the range of 95% prediction bands (Fig. 6b).

However, some other factors might also affect the evaluation process, such as specific types of DOM molecules, pH of samples. A less negative ζ potential of Fe-MNPs was observed for RW, although it contained relatively higher level of DOM and the least abundance of metal cations. It has been reported that organism-originated organic molecules, such as amino acids, aldehydes and mono-carboxylic acids occur in rainfall (Balla et al., 2014; Ćosović et al., 2007; Muller et al., 2008). In this study, significant fluorescence peaks associated with amino acid- and protein-like molecules of RW were also observed at λ_{Ex} 296 and λ_{Em} 370 nm (Fig. 7c). Because of possessing both positively and negatively charged functional groups, the amino acid- and protein-like molecules adsorbed on Fe-MNPs without bridging by metal cations, and thus affected the ζ potentials of Fe-MNPs much less. Therefore, DOM adsorbed on Fe-MNPs in the sample of RW was 39.47 ± 6.98 mg/L, but the adsorbed concentration of metal cations was totally 0.06 ± 0.15 mM pH was another factor to affect surface charges of Fe-MNPs. At pH 5.0, the sign of the ζ potential of Fe-MNPs was reversed to positive for some samples, with the greatest change for the sample of rainwater,

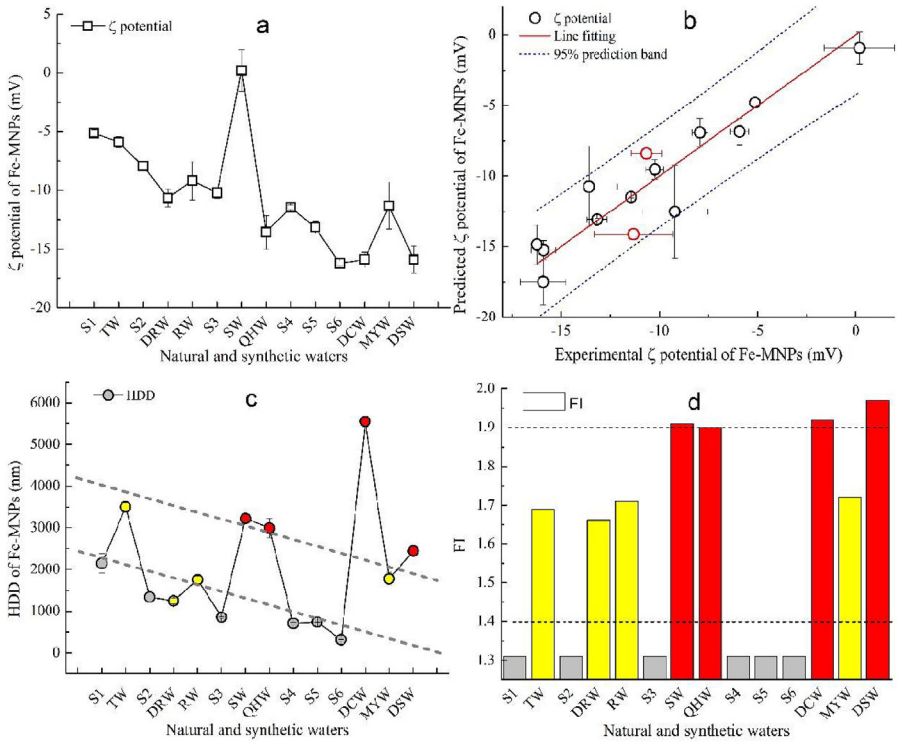

Fig. 6. Experimental ζ potential (a), fitting curve (b), HDD (c) of Fe-MNPs at pH 7.0 and FI of 14 waters (d).

Table 1
Parameters of waters and Fe-MNPs at pH 7.0.

Samples[a]	pH	TOC (mg/L)	I_c[b]	FI[c]	ζ potential (mV) (pH 7.0)	DOM (TOC) (mg/g)	Cations (mM/g)
TW	6.76 ± 0.13	2.00 ± 0.05	3.45 ± 0.01	1.69	−5.91 ± 0.45	3.87 ± 2.20	8.00 ± 3.13
DRW	7.39 ± 0.17	3.40 ± 0.04	3.21 ± 0.04	1.66	−10.66 ± 0.76	29.00 ± 2.22	8.00 ± 3.99
RW	6.80 ± 0.15	4.31 ± 0.27	0.32 ± 0.00	1.71	−9.21 ± 1.65	39.47 ± 6.98	0.06 ± 0.15
SW	6.90 ± 0.04	7.21 ± 0.40	2412.72 ± 17.27	1.91	0.19 ± 1.79	7.93 ± 8.77	33.04 ± 5.54
QHW	6.72 ± 0.21	8.36 ± 0.07	4.04 ± 0.09	1.90	−13.58 ± 1.45	81.20 ± 7.83	11.64 ± 1.48
DCW	6.84 ± 0.06	31.21 ± 0.00	2.33 ± 0.00	1.92	−15.90 ± 0.62	79.67 ± 2.32	5.47 ± 1.06
MYW	7.12 ± 0.11	32.71 ± 0.10	5.06 ± 0.08	1.72	−11.31 ± 2.01	87.60 ± 5.15	2.84 ± 1.67
DSW	6.56 ± 0.03	97.64 ± 0.07	4.64 ± 0.08	1.97	−15.91 ± 1.15	158.87 ± 18.53	7.38 ± 2.60
S1	7.01 ± 0.04	1.58 ± 0.12	9.01 ± 0.07	1.31	−5.13 ± 0.26	21.25 ± 0.43	15.39 ± 1.41
S2	6.89 ± 0.03	2.97 ± 0.08	6.99 ± 0.05	1.31	−7.93 ± 0.40	32.73 ± 1.08	18.87 ± 2.76
S3	7.05 ± 0.01	5.57 ± 0.24	4.00 ± 0.08	1.31	−10.23 ± 0.45	37.16 ± 0.67	24.50 ± 4.01
S4	7.01 ± 0.02	10.36 ± 0.19	3.52 ± 0.11	1.31	−11.43 ± 0.21	45.49 ± 0.28	29.79 ± 3.43
S5	7.00 ± 0.07	15.44 ± 0.71	2.51 ± 0.03	1.31	−13.17 ± 0.50	60.08 ± 1.33	23.21 ± 0.58
S6	6.97 ± 0.05	20.19 ± 0.58	1.24 ± 0.05	1.31	−16.23 ± 0.23	78.46 ± 0.11	12.04 ± 0.79

[a] TW is for tap water; DRW for Dari river water; RW for rainwater; SW for seawater; QHW for Qinghe river water; DCW for Dianchi river water; MYW for Muyun reservoir water; DSW for domestic sewage water; S1 ~ S6 for six synthetic water samples.
[b] Cationic strength (I_c) was calculated with $\frac{1}{2}\sum z_i^2 c_i$, Z_i and C_i were the valence state and molar concentration (mol/m^3, M) of *i* cation separately.
[c] Fluorescence index (FI) was the ratio of fluorescence intensity of λ_{Em} 450 nm to that of 500 nm at λ_{Ex} 370 nm.

Table 2
Parameters and fitting equations to predict ζ potential of Fe-MNPs as a function of pH.

pH of samples	Fitting equations[a]	Adj. R^2	S.E.[b]	*F*	*P*[c]
7.0	$y=(3.36\pm0.58)\lg x_1-(6.50\pm1.03)\lg x_2-(6.69\pm1.19)$	0.880	1.75	41.31	0.000
9.0	$y=(4.75\pm0.56)\lg x_1-(4.97\pm1.01)\lg x_2-(10.16\pm1.16)$	0.903	1.72	52.12	0.000
5.0	$y=(-12.54\pm3.10)lgx_1-(11.38\pm2.08)lgx_2+(14.62\pm2.71)$	0.718	13.11	15.00	0.001

[a] y is the predicted ζ potential of Fe-MNPs; x_1 is I_c of each water; x_2 is TOC of each water.
[b] Standard error (S.E.) was calculated with $[\Sigma(y-y^*)^2/(n-3)]^{1/2}$, y^* was the experimental ζ value.
[c] *P* statistical significance level.

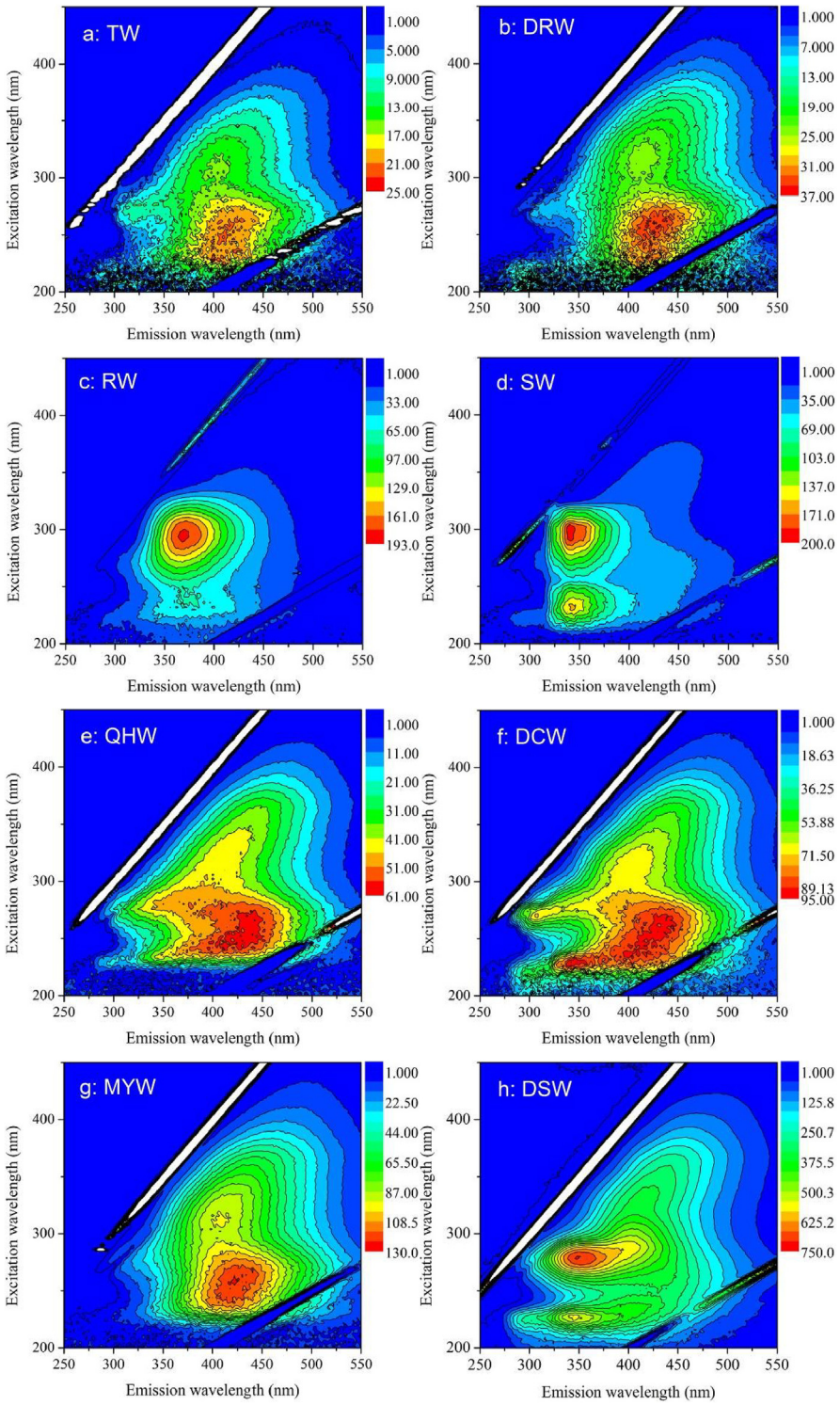

Fig. 7. Excitation-emission fluorescence spectra of eight environmental waters.

followed by tap water (Table S5). One possible explanation is that hydrogen possessed a greater affinity for functional groups of Fe-MNPs or negatively charged functional groups of organic molecules, both of which hindered DOM molecules bonding to Fe-MNPs by competitive adsorption (Piccolo et al., 2003). As a result, due to intervention of hydrogen, the R^2 for pH 5.0 was only 0.718, while a greater R^2 of 0.903 was obtained for pH 9.0 (Table 2).

For the combination of all 14 synthetic and environmental water samples studied, we observed that the change of HDD of Fe-MNPs indeed associated well with the ζ potential of the particle when concentrations of DOM were relatively less. However, for greater concentrations of DOM, HDD of Fe-MNPs was unexpectedly larger, although the negative ζ potential of particles was strengthened by the presence of adsorbed DOM, especially for QHW and DCW compared with synthetic waters (Fig. 6c). Waters from the QH River and DC Lake were contaminated by domestic sewage, and

significant peaks of fluorescence spectra for amino acid- and protein-like molecules were also observed in both waters, which could hinder metal cations bridging between the organic macromolecules adsorbed on Fe-MNPs (Fig. 7e–f) (Chen et al., 2003; Ma and Wang, 2015). In the sample from DSW the larger amount of DOM stabilized repulsion between particles, although the amount of DOM (158.9 mg/g) and metal cations (7.4 mM/g) adsorbed on Fe-MNPs were relatively larger compared to the other water samples (Table 1). It has been proposed that electrosteric stabilization was responsible for this difference (Alsudir and Lai, 2017). Due to greater adsorption of various DOM molecules and metal cations, the thickness of the adsorbed layer around Fe-MNPs was larger than the Debye length so that van der Waals forces were less dominant than electrostatic repulsion between particles, which resulted in restablization of Fe-MNPs (Philippe and Schaumann, 2014; Tiller and O'Meila, 1993). In addition, the ratio (fluorescence index, FI) of intensity of λ_{Em} 450 nm to that of 500 nm at λ_{Ex} 370 nm is generally used for distinguishing among relative contributions of DOMs from various sources (Zhang and He, 2015). A value of FI greater than 1.9 indicates that DOM is comprised primarily of molecules of microbial origin (fresh DOM). Values of 1.4 or less suggest that DOM is of terrestrial origin (decomposed DOM) (McKnight et al., 2001). The FI of SW, QHW, DCW and DSW were greater than 1.9, which indicates DOM derived from microorganisms (fresh DOM) (Zhang and He, 2015), thus should contain amino acid- and protein-like biomass molecules. With the decomposition of DOM, waters with lower FI increased the HDD of Fe-MNPs much less (aged DOM) (Fig. 6c–d). Consequently, to accurately evaluate the stability of Fe-MNPs in environmental waters, it is necessary to identify specific interactions of Fe-MNPs with different types of DOM and cations under complex conditions.

4. Conclusions

Aggregation and suspension of Fe-MNPs in environmental waters are complex and affected by concentrations and types of DOM and metal cations as well as pH conditions. Observations derived from this study indicated that: (1) per the synthetic water experiment, bridging complexation effect of Ca^{2+}, Mg^{2+} largely promoted multilayer adsorption of DOM molecules on Fe-MNPs and caused greater aggregation of Fe-MNPs compared with Na^{+}. (2) Demonstrated with the "real world" environmental water samples, ζ potentials of Fe-MNPs in environmental waters could be well evaluated by using concentration of DOM and I_c, and an excellent correlation was observed between predicted values and experiment values ($R^2 = 0.880$). (3) Amino acid- and protein-like molecules in environmental waters (e.g., urban river) largely increased the aggregation of Fe-MNPs due to their ampholytic characteristics. In addition, data obtained in this work showed that waters with relatively greater concentrations of DOM (e.g. domestic sewage) tended to minimize aggregation of Fe-MNPs due to electrosteric effects. The above interactions affected the colloidal stability of Fe-MNPs jointly, which complicated evaluating the colloidal stability of Fe-MNPs in a short period. Therefore, long-term behaviors of the particles in multi-component systems should be paid more attention. These findings are useful for revealing the interaction of nanomaterials with water components and assessing their risks in environmental waters.

Acknowledgements

This work was supported by the National Natural Science Foundation of China (No.41222026, 41630645, 41673131).

Appendix A. Supplementary data

Supplementary data related to this article can be found at https://doi.org/10.1016/j.envpol.2018.06.029.

References

Abate, G., Masini, J.C., 2001. Acid-basic and complexation properties of a sedimentary humic acid. A study on the Barra Bonita reservoir of Tietê river, São Paulo State, Brazil. J. Braz. Chem. Soc. 12, 109–116.
Aiken, G.R., Hsu-Kim, H., Ryan, J.N., 2011. Influence of dissolved organic matter on the environmental fate of metals, nanoparticles, and colloids. Environ. Sci. Technol. 45 (8), 3196–3201.
Alsudir, S., Lai, E.P.C., 2017. Electrosteric stabilization of colloidal TiO2 nanoparticles with DNA and polyethylene glycol for selective enhancement of UV detection sensitivity in capillary electrophoresis analysis. Anal. Bioanal. Chem. 409 (7), 1857–1868.
Amarasiriwardena, D., Siripinyanond, A., Barnes, R.M., 2001. Trace elemental distribution in soil and compost-derived humic acid molecular fractions and colloidal organic matter in municipal wastewater by flow field-flow fractionation-inductively coupled plasma mass spectrometry (flow FFF-ICP-MS). J. Anal. At. Spectrom 16 (9), 978–986.
Amde, M., Liu, J.-f., Tan, Z.-Q., Bekana, D., 2017. Transformation and bioavailability of metal oxide nanoparticles in aquatic and terrestrial environments. A review. Environ. Pollut. 230, 250–267.
Balla, D., Papageorgiou, A., Voutsa, D., 2014. Carbonyl compounds and dissolved organic carbon in rainwater of an urban atmosphere. Environ. Sci. Pollut. Res. 21 (20), 12062–12073.
Bian, S.W., Mudunkotuwa, I.A., Rupasinghe, T., Grassian, V.H., 2011. Aggregation and dissolution of 4 nm ZnO nanoparticles in aqueous environments: influence of pH, ionic strength, size, and ddsorption of humic acid. Langmuir 27 (10), 6059–6068.
Boström, M., Williams, D.R.M., Ninham, B.W., 2001. Specific ion effects: why DLVO theory fails for biology and colloid systems. Phys. Rev. Lett. 87 (16), 168103.
Chen, W., Westerhoff, P., Leenheer, J.A., Booksh, K., 2003. Fluorescence excitation–emission matrix regional integration to quantify spectra for dissolved organic matter. Environ. Sci. Technol. 37 (24), 5701–5710.
Ćosović, B., Orlović Leko, P., Kozarac, Z., 2007. Rainwater dissolved organic carbon: characterization of surface active substances by electrochemical method. Electroanalysis 19 (19–20), 2077–2084.
Dong, H., Ahmad, K., Zeng, G., Li, Z., Chen, G., He, Q., Xie, Y., Wu, Y., Zhao, F., Zeng, Y., 2016. Influence of fulvic acid on the colloidal stability and reactivity of nanoscale zero-valent iron. Environ. Pollut. 211, 363–369.
Erhayem, M., Sohn, M., 2014. Stability studies for titanium dioxide nanoparticles upon adsorption of Suwannee River humic and fulvic acids and natural organic matter. Sci. Total Environ. 468–469 (4), 249–257.
Filius, J.D., Lumsdon, D.G., Meeussen, J.C.L., Hiemstra, T., Van Riemsdijk, W.H., 2000. Adsorption of fulvic acid on goethite. Geochem. Cosmochim. Acta 64 (1), 51–60.
Filius, J.D., Meeussen, J.C.L., Lumsdon, D.G., Hiemstra, T., van Riemsdijk, W.H., 2003. Modeling the binding of fulvic acid by goethite: the speciation of adsorbed FA molecules. Geochem. Cosmochim. Acta 67 (8), 1463–1474.
Ghosh, S., Jiang, W., McClements, J.D., Xing, B., 2011. Colloidal stability of magnetic iron oxide nanoparticles: influence of natural organic matter and synthetic polyelectrolytes. Langmuir 27 (13), 8036–8043.
Ghosh, S., Mashayekhi, H., Pan, B., Bhowmik, P., Xing, B., 2008. Colloidal behavior of aluminum oxide nanoparticles as affected by pH and natural organic matter. Langmuir 24 (21), 12385–12391.
Ghosh, S., Pradhan, N.R., Mashayekhi, H., Dickert, S., Thantirige, R., Tuominen, M.T., Tao, S., Xing, B., 2014. Binary short-range colloidal assembly of magnetic iron oxides nanoparticles and fullerene (nC60) in environmental media. Environ. Sci. Technol. 48 (20), 12285–12291.
Godinez, I.G., Darnault, C.J.G., 2011. Aggregation and transport of nano-TiO2 in saturated porous media: effects of pH, surfactants and flow velocity. Water Res. 45 (2), 839–851.
Gottschalk, F., Sun, T., Nowack, B., 2013. Environmental concentrations of engineered nanomaterials: review of modeling and analytical studies. Environ. Pollut. 181, 287–300.
Guo, K., Han, F.X., Kingery, W., Sun, H., Zhang, J., 2016. Development of novel nanomaterials for remediation of heavy metals and radionuclides in contaminated water. Nanotechnol. Environ. Eng 1 (1), 7.
He, Z., Cao, X., Mao, J., Ohno, T., Waldrip, H.M., 2013. Analysis of carbon functional groups in mobile humic acid and recalcitrant calcium humate extracted from eight US soils. Pedosphere 23, 705–716.
He, Z., Ohno, T., Cade-Menun, B.J., Erich, M.S., Honeycutt, C.W., 2006. Spectral and chemical characterization of phosphates associated with humic substances. Soil Sci. Soc. Am. J. 70 (5), 1741–1751.
He, Z., Ohno, T., Olk, D.C., Wu, F., 2010. Capillary electrophoresis profiles and fluorophore components of humic acids in Nebraska corn and Philippine rice soils. Geoderma 156, 143–151.
He, Z., Ohno, T., Wu, F., Olk, D.C., Honeycutt, C.W., Olanya, M., 2008. Capillary electrophoresis and fluorescence excitation-emission matrix spectroscopy for characterization of humic substances. Soil Sci. Soc. Am. J. 72 (5), 1248–1255.
Johnson, R.L., Johnson, G.O.B., Nurmi, J.T., Tratnyek, P.G., 2009. Natural organic

matter enhanced mobility of nano zerovalent Iron. Environ. Sci. Technol. 43 (14), 5455–5460.
Kunz, W., 2010. Specific Ion Effects. World Scientific, Singapore, pp. 3–54.
Leenheer, J.A., Wershaw, R.L., Reddy, M.M., 1995. Strong-acid, carboxyl-group structures in fulvic acid from the Suwannee River, Georgia. I: Minor structures. Environ. Sci. Technol. 29 (2), 393–398.
Lei, C., Sun, Y., Tsang, D.C.W., Lin, D., 2018. Environmental transformations and ecological effects of iron-based nanoparticles. Environ. Pollut. 232, 10–30.
Liu, S., Zhu, Y., Liu, L., He, Z., Giesy, J.P., Bai, Y., Sun, F., Wu, F., 2018. Cation-induced coagulation of aquatic plant-derived dissolved organic matter: investigation by EEM-PARAFAC and FT-IR spectroscopy. Environ. Pollut. 234, 726–734.
Luna-Valdez, J.G., Balandran-Quintana, R.R., Azamar-Barrios, J.A., Ramos Clamont-Montfort, G., Mendoza-Wilson, A.M., Mercado-Ruiz, J.N., Madera-Santana, T.J., Rascon-Chu, A., Chaquilla-Quilca, G., 2017. Structural and physicochemical characterization of nanoparticles synthesized from an aqueous extract of wheat bran by a cold-set gelation/desolvation approach. Food Hydrocolloids 62, 165–173.
Ma, G., Wang, S., 2015. Temporal and spatial distribution changing characteristics of exogenous pollution load into Dianchi Lake, Southwest of China. Environ. Earth Sci. 74 (5), 3781–3793.
McKnight, D.M., Boyer, E.W., Westerhoff, P.K., Doran, P.T., Kulbe, T., Andersen, D.T., 2001. Spectrofluorometric characterization of dissolved organic matter for indication of precursor organic material and aromaticity. Limnol. Oceanogr. 46 (1), 38–48.
Muller, C.L., Baker, A., Hutchinson, R., Fairchild, I.J., Kidd, C., 2008. Analysis of rainwater dissolved organic carbon compounds using fluorescence spectrophotometry. Atmos. Environ. 42 (34), 8036–8045.
Newville, M., 2001. IFEFFIT: interactive XAFS analysis and FEFF fitting. J. Synchrotron Radiat. 8, 322–324.
Ohno, T., He, Z., Sleighter, R.L., Honeycutt, C.W., Hatcher, P.G., 2010. Ultrahigh resolution mass spectrometry and indicator species analysis to identify marker components of soil- and plant biomass-derived organic matter fractions. Environ. Sci. Technol. 44, 8594–8600.
Paul, S., Sharma, T., Saikia, D., Saikia, P., Borah, D., Baruah, M., 2015. Evaluation of pKa values of soil humic acids and their complexation properties. Int. J. Plant Soil Sci. 6 (4), 218–228.
Philippe, A., Schaumann, G.E., 2014. Interactions of dissolved organic matter with natural and engineered inorganic colloids: a review. Environ. Sci. Technol. 48 (16), 8946–8962.
Piccolo, A., Conte, P., Spaccini, R., Chiarella, M., 2003. Effects of some dicarboxylic acids on the association of dissolved humic substances. Biol. Fertil. Soils 37 (4), 255–259.
Ravel, B., Newville, M., 2005. ATHENA, ARTEMIS, HEPHAESTUS: data analysis for X-ray absorption spectroscopy using IFEFFIT. J. Synchrotron Radiat. 12, 537–541.
Reddy, L.H., Arias, J.L., Nicolas, J., Couvreur, P., 2012. Magnetic nanoparticles: design and characterization, toxicity and biocompatibility, pharmaceutical and biomedical applications. Chem. Rev. 112 (11), 5818–5878.
Rossi, L.M., Costa, N.J.S., Silva, F.P., Wojcieszak, R., 2014. Magnetic nanomaterials in catalysis: advanced catalysts for magnetic separation and beyond. Green Chem. 16 (6), 2906–2933.
Saleh, N., Kim, H.J., Phenrat, T., Matyjaszewski, K., Tilton, R.D., Lowry, G.V., 2008. Ionic strength and composition affect the mobility of surface-modified Fe0 nanoparticles in water-saturated sand columns. Environ. Sci. Technol. 42 (9), 3349–3355.
Taghiyari, H.R., Norton, J., Tajvidi, M., 2017. Effects of nano-materials on different properties of wood-composite materials. In: He, Z. (Ed.), Bio-based Wood Adhesives: Preparation, Characterization, and Testing. CRC Press, Boca Raton, Fl, pp. 310–339.
Tiller, C.L., O'Melia, C.R., 1993. Natural organic matter and colloidal stability: models and measurements. Colloids Surf., A 73, 89–102.
Vindedahl, A.M., Strehlau, J.H., Arnold, W.A., Penn, R.L., 2016. Organic matter and iron oxide nanoparticles: aggregation, interactions, and reactivity. Environ. Sci. Nano 3 (3), 494–505.
Wang, H., Zhao, X., Han, X., Tang, Z., Liu, S., Guo, W., Deng, C., Guo, Q., Wang, H., Wu, F., Meng, X., Giesy, J.P., 2017. Effects of monovalent and divalent metal cations on the aggregation and suspension of Fe_3O_4 magnetic nanoparticles in aqueous solution. Sci. Total Environ. 586, 817–826.
Wang, H., Zhao, X., Meng, W., Wang, P., Wu, F., Tang, Z., Han, X., Giesy, J.P., 2015. Cetyltrimethylammonium bromide-coated Fe_3O_4 magnetic nanoparticles for analysis of 15 Trace polycyclic aromatic hydrocarbons in aquatic environments by ultraperformance, liquid chromatography with fluorescence detection. Anal. Chem. 87 (15), 7667–7675.
Wiesner, M.R., Lowry, G.V., Alvarez, P., Dionysiou, D., Biswas, P., 2006. Assessing the risks of manufactured nanomaterials. Environ. Sci. Technol. 40 (14), 4336–4345.
Wu, F., Mu, Y., Chang, H., Zhao, X., Giesy, J.P., Wu, K.B., 2013. Predicting water quality criteria for protecting aquatic life from physicochemical properties of metals or metalloids. Environ. Sci. Technol. 47 (1), 446–453.
Xia, T., Qi, Y., Liu, J., Qi, Z., Chen, W., Wiesner, M.R., 2017. Cation-inhibited transport of graphene oxide nanomaterials in saturated porous media: the Hofmeister effects. Environ. Sci. Technol. 51 (2), 828–837.
Yang, K., Xing, B.S., 2009. Adsorption of fulvic acid by carbon nanotubes from water. Environ. Pollut. 157 (4), 1095–1100.
Zhang, M., He, Z., 2015. Characteristics of dissolved organic carbon revealed by ultraviolet–visible absorbance and fluorescence spectroscopy: the current status and future exploration. In: He, Z., Wu, F. (Eds.), Labile Organic Matter - Chemical Compositions, Function, and Significance in Soil and the Environment. SSSA Special Publication 62. Soil Sci. Soc. Am., Madison, WI, pp. 1–22.
Zhao, J., Wang, Z., Dai, Y., Xing, B., 2013. Mitigation of CuO nanoparticle-induced bacterial membrane damage by dissolved organic matter. Water Res. 47 (12), 4169–4178.
Zhao, X., Shi, Y., Cai, Y., Mou, S., 2008. Cetyltrimethylammonium bromide-coated magnetic nanoparticles for the preconcentration of phenolic compounds from environmental water samples. Environ. Sci. Technol. 42 (4), 1201–1206.
Zhu, S., Xue, M.Y., Luo, F., Chen, W.C., Zhu, B., Wang, G.X., 2017. Developmental toxicity of Fe3O4 nanoparticles on cysts and three larval stages of Artemia salina. Environ. Pollut. 230, 683–691.

Supporting Information

Colloidal Stability of Fe_3O_4 Magnetic Nanoparticles Differentially Impacted by Dissolved Organic Matter and Cations in Synthetic and Naturally-Occurred Environmental Waters

Hao Wang[a,b], Xiaoli Zhao[a,*], Xuejiao Han[a], Zhi Tang[a], Fanhao Song[a], Shaoyang Zhang[c], Yuanrong Zhu[a], Wenjing Guo[a], Zhongqi He[d], Qingwei Guo[b], Fengchang Wu[a], Xiaoguang Meng[e], John P. Giesy[a,f]

[a] *State Key Laboratory of Environmental Criteria and Risk Assessment, Chinese Research Academy of Environmental Sciences, Beijing 100012, China.*

[b] *South China Institute of Environmental Sciences, Ministry of Environmental Protection, Guangzhou, China.*

[c] *College of Geoscience and Surveying Engineering, China University Mining and Technology, Beijing 100083, China.*

[d] *USDA-ARS Southern Regional Research Center, 1100 Robert E Lee Blvd, New Orleans, LA 70124, USA.*

[e] *Center for Environmental Systems, Stevens Institute of Technology, Hoboken, New Jersey 07030, United States*

[f] *Department of Biomedical and Veterinary Biosciences and Toxicology Centre, University of Saskatchewan, Saskatoon, Saskatchewan, Canada.*

*Corresponding Authors: zhaoxiaoli_zxl@126.com.

Tel.: (+86)10-84931804; Fax: (+86)10-84931804.

This supporting information contains 6 tables and 5 figures. This document contains 18 pages including this cover page.

Method and Materials:

Synthetic waters: In the study, 6 waters were synthesized with Na^{+}, Mg^{2+}, Ca^{2+} and FA (Table S6).

Kinetic adsorption of FA and HA. Kinetics of adsorption of FA and HA on surfaces of Fe-MNPs were fitted by use of pseudo-first-order (PFO) (Equation 1) and pseudo-second-order (PSO) (Equation 2) models, respectively.

$$\ln(q_e - q_t) = \ln q_e - k_1 t \quad (1)$$

$$\frac{t}{q_t} = \frac{1}{k_2 q_e^2} + \frac{t}{q_e} \quad (2)$$

Where: q_e and q_t are the amounts of adsorbate per united adsorbent at equilibrium and time t, respectively. k_1 and k_2 are rate constants of PFO and PSO models, respectively.

Statistical analysis. In the study, the Leave-one-out cross validation (LOO-CV) approach was used to estimate the performance of the developed model. Generally, estimating the potential error for each water samples by using the other water samples could reflect the performance of the model more accurately compared with the other cross validation methods (such as, Hold-out method, K-fold cross validation), which ensured the LOO-CV approach more credible and avoid effect of random factors on model development.

Results and discussion

3.1 Adsorption of FA and HA on Fe-MNPs

Adsorption of FA and HA on Fe-MNPs presented similar trends but different extent among pHs (Figure S2a-b). Due to great surface area of Fe-MNPs, adsorptions of both FA and HA were rapid and reached 80.4 and 90.2% of their maximum adsorptions respectively after 1.0 *h* at pH 5.0. The PSO model was fitted better than

the PFO model (Table S2), which means the amount of adsorption sites on particles limiting the adsorption processes of FA and HA. At pH 5.0, FA reached 90% of its maximum adsorption in 3.5 *h*, however, it took an additional 15.0 *h* to reach 98% of maximum. It indicates a slow adsorption followed the initial faster adsorption of FA and HA on Fe-MNPs, which might be attributed to more interstices between nanoparticles that reduced FA and HA molecules binding to active sites of Fe-MNPs (Ho, 2006; Qiu et al., 2009).

Adsorption efficiencies of FA and HA on Fe-MNPs were negatively proportional to pH values. Charges carried by Fe-MNPs were gradually reversed from positive to negative while the $Fe\text{-}OH_2^+$ on the surface at pH 5.0 was gradually deprotonated to form $Fe\text{-}O^-$ with the pH increasing (Hu et al., 2010; Illés et al., 2006). pH-dependent adsorptions of FA and HA were seemly attributed to electrostatic interactions between Fe-MNPs and the both organic fractions. Actually, it was found that the carboxyl group of DOM could bond to Fe^{3+} or Fe^{2+} of the particle surface to form inner sphere complex by replacing the previous adsorbed hydroxyl group (Filius et al., 2000; Filius et al., 2003). Such reaction could possibly be weakened with pH increasing due to the deprotonation of hydroxyl groups on particle surface and increase of free hydroxyl ions in solution. Therefore, ligand exchange process of carboxyl group might be originally involved in the adsorptions of FA and HA on Fe-MNPs. The result is consistent with previous findings for adsorption of HA on goethite, nano-TiO_2, ZnO and Al_2O_3 particles (Gu et al., 1994; Kun et al., 2009).

However, adsorption of HA was greater and faster than that of FA based on rate

constants (k) and initial adsorption rates (v_0) in all pH ranges (Table S2). Given relatively higher contents of phenolic and aliphatic species and lower contents of carbonyl and carboxyl species for HA molecules, HA is relatively more hydrophobic compared with FA (Table S3). Under the effects of ligand exchange or electrostatic force as well as hydrophobic force, HA molecules could adsorb on Fe-MNPs more heavily. The result is consistent with previous observations that HA has a greater affinity to nano-TiO_2 or SiO_2 particles than FA due to its less solubility, larger molecular weight and greater hydrophobicity (Erhayem et al., 2014; Liang et al., 2011). However, with pH increasing, HA molecules became more hydrophilic because of deprotonation of their carboxyl groups, which partly reduced the contribution of hydrophobic interaction. It is noteworthy that the adsorptions of FA and HA were still observed at pH 9.0, which might be ascribed to some other interaction between DOM and particles. For instance, DOM molecules adsorbed onto goethite particle also by forming H-bond between hydroxyl group of DOM and $Fe\text{-}O^-$ at high pH (Filius et al., 2000; Philippe et al., 2014). Therefore, due to the heterogeneity of DOM molecules, the interaction between DOM and Fe-MNPs is much more complex. Theoretically, molecules of DOM could bind to the Fe ion on the surface of Fe-MNPs by H-Bonding and ligand exchange to develop monolayer adsorption or by hydrophobic interaction to develop multilayer adsorption or by both effects (Dandan et al., 2016; Kondo et al., 2006). Specific mechanisms for FA and HA binding to Fe-MNPs could be identified by their adsorption types and effects on stability of Fe-MNPs.

3.2 Adsorption of metal cations on Fe-MNPs in the presence of FA and HA

Concentrations of Mg^{2+} and Ca^{2+} required for adsorption equilibrium of FA and HA were approximately 1.0 mM but Na^{+} had no effect. The possible reasons for this are that significant aggregation of Fe-MNPs at concentrations of divalent cations greater than 1.0 mM decreased surface areas of particles, which limited continuous adsorption of DOM. In contrast, due to the relatively less aggregation of Fe-MNPs adsorption of HA increased gradually as a function of concentration of Na^{+}. For the same reason, due to the small size of metal cations, amounts of metal cations adsorbed to Fe-MNPs were proportional to concentrations of metal cations, and never affected by aggregation of Fe-MNPs (Figure S3c-d). Although Ca^{2+} enhanced adsorption of HA or FA more than did Mg^{2+}, the amount of Ca^{2+} adsorbed was generally less than that of Mg^{2+}. due to its lesser affinity for carboxylic groups compared with Ca^{2+}, greater concentrations of Mg^{2+} are needed for binding to HA or FA molecules to form clusters around Fe-MNPs (Speight, 2005). Therefore, a certain number of adsorbed Mg^{2+} might have bound carboxyl groups as $COO^{-}\cdots Mg^{2+}$ instead of $COO^{-}\cdots Mg^{2+}\cdots COO^{-}$. As a result, the amount of Mg^{2+} adsorbed exceeded that of Ca^{2+}.

3.3 Effect of HA on magnetic properties of Fe-MNPs

SQUID was used to characterize the magnetic properties of HA-modified Fe-MNPs (Fig. S5). Results showed that the blocking temperatures (T_B) of pure and HA-modified (100 mg HA/L) Fe-MNPs powders were 129.13±0.99 K, 123.64±1.28

K for pH 9.0, 112.13±2.15 K for pH 7.0 and 108.63±1.87 for pH 5.0 respectively (Fig. S5a). Generally, the adsorption of HA resulted in T_B decrease of Fe-MNPs. In addition, the T_B value of Fe-MNPs decreased slightly with adsorption amounts of HA on particles increasing. Theoretically, small particles generally have lower T_B values than the larger ones due to the former having a relatively smaller volume and lower energy barrier (Goya and Morales, 2004). The above results indicated that adsorption of HA promoted the dispersion of Fe-MNPs. In addition, as shown in Fig. S5b, it did not present any magnetic hysteresis for all samples. Moreover, the HA-modified Fe-MNPs generally presented larger magnetic moments compared with the pure one. The results might indicate that the adsorption of HA could generally strengthen the dispersion and magnetism of Fe-MNPs. However, it was observed that the magnetic moments of Fe-MNPs gradually decreased as the amounts of HA adsorbed on particles increased at lower pH values. Actually, the ζ potential and HDD of Fe-MNPs presented no significant difference between pH 5.0, 7.0 and 9.0 when concentration of HA was more than 100 mg/L (Fig. 1a and b). Therefore, the effect of magnetic property of HA-modified Fe-MNPs on colloid behavior of particles might be very weak, and electrostatic and van der Waals forces dominated the process.

Table S1 Parameters of Langmuir and Freundlich fitting for FA and HA adsorption on Fe-MNPs.

DOM	pH	Langmuir fitting			Freundlich fitting		
		K_L	q_m	R^2	K_F	n	R^2
HA	5.0	7.60±3.67	155.12±11.45	0.89	97.91±6.60	5.73±0.84	0.98
	7.0	0.40±0.07	177.97±7.54	0.98	50.56±6.22	2.76±0.32	0.94
	9.0	0.34±0.09	126.79±8.33	0.97	42.54±7.36	3.38±0.66	0.90
FA	5.0	5.47±1.10	123.20±5.18	0.97	73.00±12.63	5.74±1.93	0.69
	7.0	0.65±0.16	120.09±5.92	0.98	50.95±6.17	4.05±0.66	0.92
	9.0	0.62±0.12	103.56±4.41	0.97	46.34±4.16	4.41±0.58	0.93

Table S2 Parameters used in the pseudo-first-order (PSO) model to describe adsorption of HA and FA on Fe-MNPs.

Adsorbate	pH	v_0 (mg/g/*h*)[a]	k (g/mg/*h*)	q_e (mg/g)	S.E.[b]	Adj.R^2
FA	5.0	203.13	0.073	52.75	1.48	0.982
	7.0	14.89	0.029	22.66	1.63	0.908
	9.0	1.71	0.022	8.82	0.64	0.999
HA	5.0	761.09	0.183	64.49	0.99	0.923
	7.0	30.46	0.050	24.68	1.16	0.933
	9.0	6.48	0.051	11.27	1.08	0.909

[a] adsorption rate (v_0) was calculated with $v_0=kq_e^2$;

[b] Standard error (S.E.) was calculated with $[\Sigma(q-q^*)^2/(n-2)]^{1/2}$, q and q^* were the experimental and the predicted amounts of the adsorbed HA or FA, respectively.

Table S3 Elemental compositions and ^{13}C NMR estimates of distribution of carbon in humic and fulvic acids.[a]

Fraction	Code	Elemental composition (%)				Carbon species from ^{13}C NMR (%)				
		C	H	O	N	Carbonyl	Carboxyl	Aromatic	Aliphatic	Phenolic
FA	1R105F	52.31	3.98	45.12	0.68	11.16	24	31	18	3.18
HA	2S101H	52.63	4.28	42.04	1.17	9.13	15	31	29	3.72

[a] collected from International Humic Substances Society.

Table S4 Parameters of environmental waters at pH 7.0 by using Leave-One-Out Cross Validation method.

Samples	Experimental value	a	b	Intercept	predicted values	Adj. R^2	*F*	*P*
TW	-5.91±0.45	-6.23±1.16	3.40±0.60	-7.08±1.39	-7.07	0.87	35.24	0.0001
RW	-9.21±1.65	-5.93±0.76	3.98±0.46	-8.05±0.95	-13.81	0.94	86.12	0.0000
SW	0.19±1.79	-6.74±0.92	1.20±1.27	-5.59±1.21	-6.98	0.85	28.43	0.0002
QHW	-13.58±1.45	-6.52±0.90	3.32±0.50	-6.40±1.05	-10.47	0.91	53.63	0.0000
DCW	-15.90±0.62	-6.35±1.15	3.34±0.61	-6.75±1.26	-15.15	0.86	32.83	0.0001
DSW	-15.91±1.15	-7.61±1.31	3.32±0.56	-5.89±1.30	-19.10	0.88	40.84	0.0001
S1	-5.00±0.36	-6.62±1.21	3.36±0.61	-6.55±1.42	-4.62	0.86	32.65	0.0001
S2	-7.73±0.95	-6.69±1.11	3.37±0.60	-6.43±1.31	-6.74	0.88	37.16	0.0001
S3	-10.33±0.42	-6.56±1.09	3.35±0.60	-6.57±1.28	-9.42	0.88	38.14	0.0001
S4	-11.43±0.40	-6.51±1.09	3.36±0.61	-6.70±1.27	-11.49	0.88	36.84	0.0001
S5	-13.201±1.01	-6.50±1.11	3.36±0.61	-6.69±1.26	-13.11	0.87	35.77	0.0001
S6	-16.43±0.55	-6.31±1.07	3.26±0.60	-6.67±1.21	-14.60	0.87	35.20	0.0001
Adj. R_{CV}^2						0.64		
Total samples		-6.50±1.03	3.36±0.58	-6.63±1.19		0.88	41.31	0.0000
R^2- R_{CV}^2						0.24＜0.3		
DRW	-10.66±0.76				-8.39			
MYW	-11.31±2.01				-14.14			

R_{CV}^2 is coefficient of determination by using the Leave-One-Out Cross Validation method, and calculated with $1 - \left[\sum_{i=1}^{n}\left(y_i^{experi} - y_i^{predcv}\right)^2\right] / \left[\sum_{i=1}^{n}\left(y_i^{experi} - \bar{y}^{experi}\right)^2\right]$.

Table S5 Parameters of 14 waters and ζ potential of Fe-MNPs at pH 5.0 and 9.0.

Samples	TOC (mg/L)		Ca^{2+} (mM)		Mg^{2+} (mM)		Na^{+} (mM)		ζ potential (mV)				HDD (nm)			
									pH 5.0		pH 9.0		pH 5.0		pH 9.0	
	value	std.	value	std.	value	std.	value	std.	value	std.	value	std.	value	std.	value	std.
TW	2.00	0.05	1.19	0.00	0.51	0.00	0.05	0.00	4.62	0.05	-7.61	1.01	3501.67	462.45	4477.83	330.22
DRW	3.40	0.04	0.79	0.01	0.79	0.01	0.06	0.00	-6.83	0.03	-8.68	0.19	1247.00	72.12	1398.00	123.04
RW	4.31	0.27	0.15	0.00	0.01	0.00	0.00	0.00	10.87	3.49	-12.67	0.61	1754.67	308.77	1972.50	430.63
SW	7.21	0.40	8.66	0.08	28.07	0.08	4668.74	33.83	0.35	1.21	2.94	1.47	3221.50	512.65	4651.50	824.72
QHW	8.36	0.07	0.97	0.02	0.87	0.02	0.31	0.01	-6.65	0.16	-14.17	1.32	2984.50	278.36	4375.50	345.78
DCW	31.21	0.00	0.57	0.00	0.53	0.00	0.09	0.00	-14.47	0.28	-16.65	0.12	5551.17	131.29	4628.67	417.66
MYW	32.71	0.10	1.56	0.02	0.87	0.02	0.24	0.01	-7.60	1.00	-9.71	0.44	1706.17	92.63	1973.00	88.62
DSW	97.64	0.07	1.33	0.02	0.73	0.01	0.39	0.01	-15.45	0.64	-15.92	0.64	2441.50	821.42	2570.33	221.56
S1	1.58	0.12	0.23	0.05	0.25	0.01	0.49	0.01	2.77	0.08	-6.78	0.38	2346.00	272.47	2146.33	234.27
S2	2.97	0.08	0.52	0.02	0.49	0.04	1.02	0.05	-5.53	0.23	-10.87	0.65	1360.67	137.17	1276.00	94.46
S3	5.57	0.24	0.51	0.04	1.03	0.06	0.97	0.07	-7.90	0.44	-11.97	0.30	917.70	137.17	620.97	14.20
S4	10.36	0.19	0.53	0.00	0.95	0.02	1.98	0.04	-9.63	0.68	-12.87	1.50	695.43	13.16	551.63	11.03
S5	15.44	0.71	2.01	0.00	1.01	0.11	2.05	0.01	-12.17	1.86	-13.90	0.20	490.13	10.18	470.30	16.63
S6	20.19	0.58	1.98	0.06	1.89	0.09	2.10	0.10	-15.00	0.10	-16.47	0.21	334.13	3.93	333.87	1.68

151 **Table S6** The concentration of FA and metal cations for synthetic waters.

Water	FA (mg/L)	Na^{+} (mM)	Mg^{2+} (mM)	Ca^{2+} (mM)
S1	2.0	2.0	2.0	2.0
S2	5.0	2.0	1.0	2.0
S3	10.0	2.0	1.0	0.5
S4	20.0	1.0	1.0	0.5
S5	30.0	1.0	0.5	0.5
S6	40.0	0.5	0.25	0.25

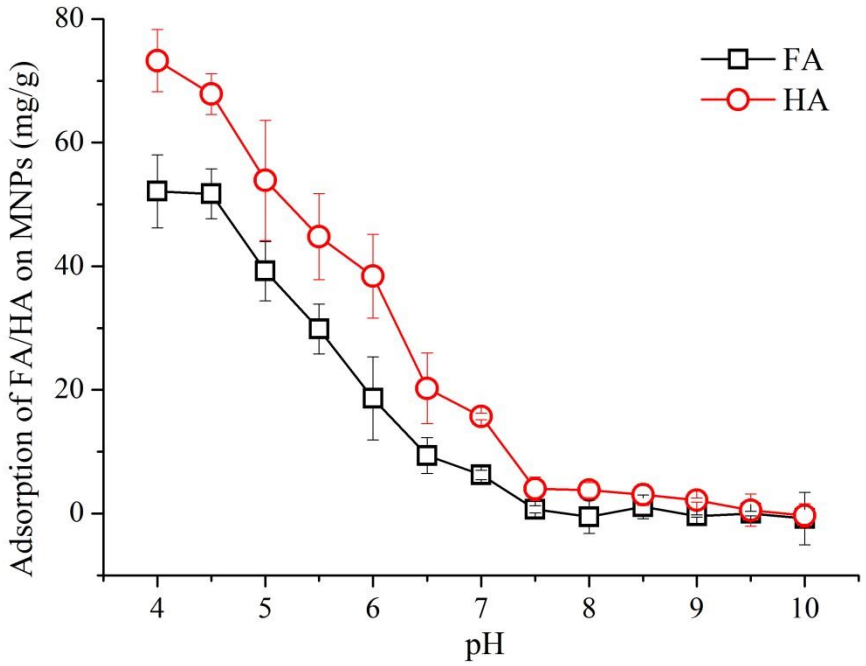

Fig. S1. Adsorptions of FA and HA (10 mg/L) on the surface of Fe-MNPs as a function of pH.

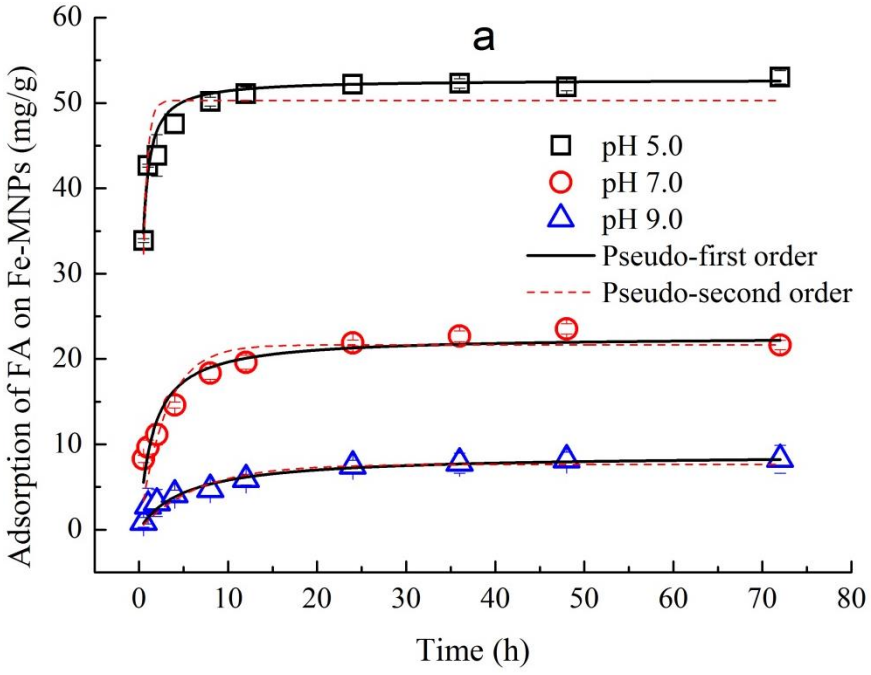

155

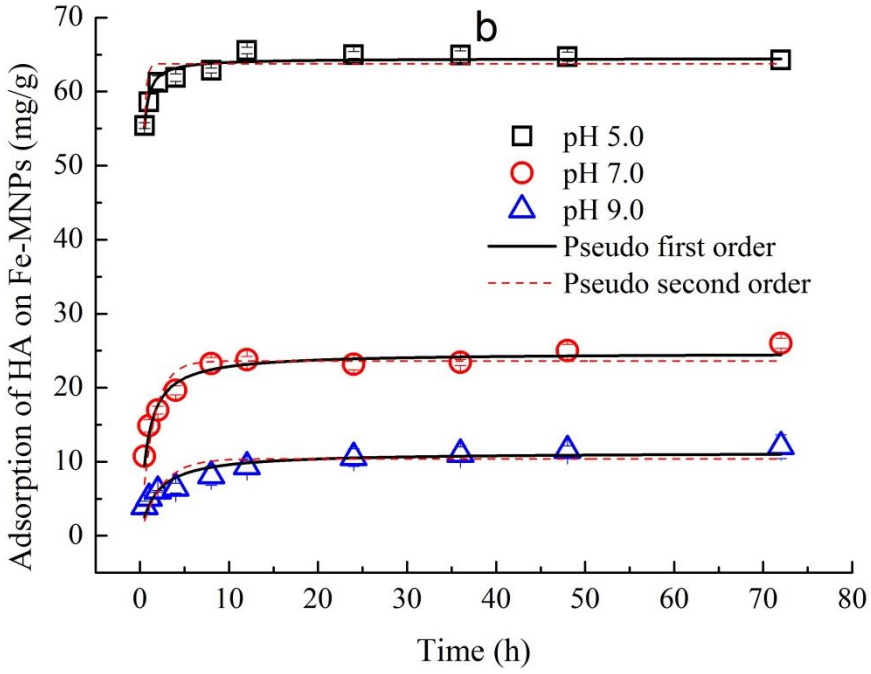

156

157 **Fig. S2.** Adsorption kinetics of FA (a) and HA (b) (10.0 mg/L) on Fe-MNPs.

158

159

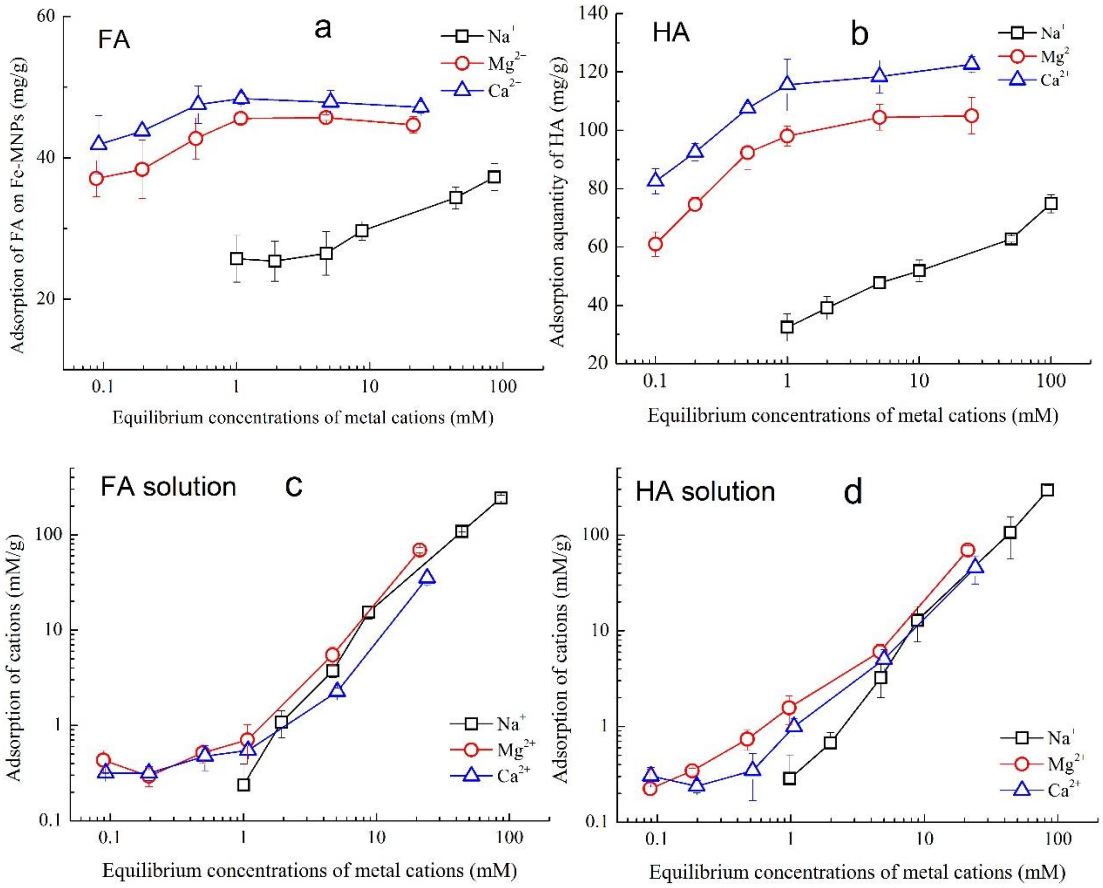

160

161 **Fig. S3.** Effects of Na^{+}, Mg^{2+} and Ca^{2+} on adsorptions of FA (a), HA (b) and metal
162 cations (c) & (d) on Fe-MNPs in 10.0 mg/L FA and HA solutions respectively.

163

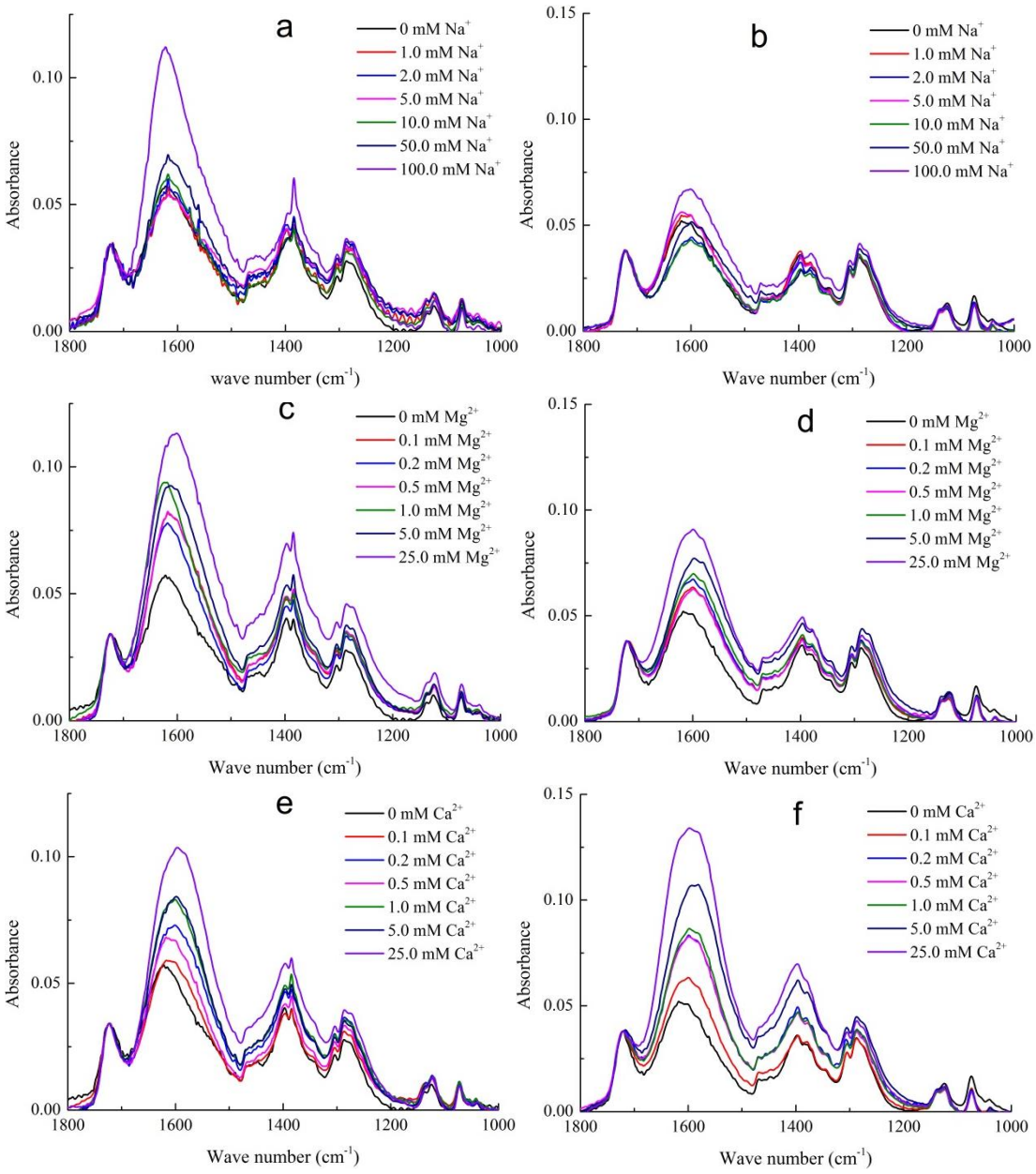

Fig. S4. Normalized FTIR spectra Fe-MNPs coated with HA/FA as functions of metal cations. 10.0 mg/L FA for Na^+ (a), Mg^{2+} (c) and Ca^{2+} (e); 10.0 mg/L HA for Na^+ (b), Mg^{2+} (d) and Ca^{2+} (f).

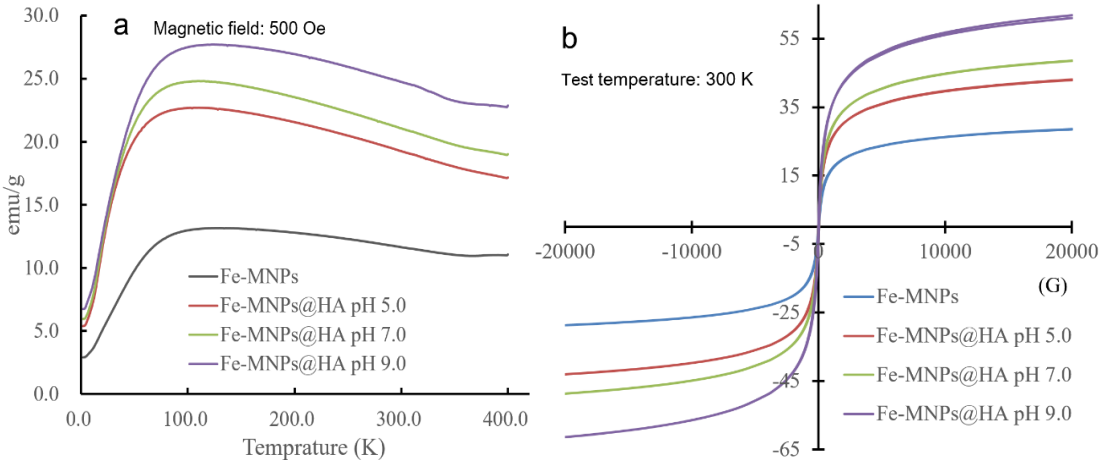

170

171 **Fig. S5.** The T_B (a) and magnetic moments (b) of pure and HA-modified Fe-MNPs

172

References

Dandan, L.I., Peng, C., Zhang, T., Qingbao, G.U., 2016. Adsorption performance of fly ash based adsorbent with fiber as pore-forming agent for dye removal. Environ. Sci. Technol.

Erhayem, M., Sohn, M., 2014. Stability studies for titanium dioxide nanoparticles upon adsorption of Suwannee River humic and fulvic acids and natural organic matter. Sci. Total. Environ. 468-469 (4), 249-257.

Filius, J.D., Lumsdon, D.G., Meeussen, J.C.L., Hiemstra, T., Van Riemsdijk, W.H., 2000. Adsorption of fulvic acid on goethite. Geochim. Cosmochim. Ac 64 (1), 51-60.

Filius, J.D., Meeussen, J.C.L., Lumsdon, D.G., Hiemstra, T., van Riemsdijk, W.H., 2003. Modeling the binding of fulvic acid by goethite: the speciation of adsorbed FA molecules. Geochim. Cosmochim. Ac 67 (8), 1463-1474.

G. F. Goya, M. P. Morales, 2004. Field dependence of blocking temperature in magnetite nanoparticles. J. Metast. Nanocrystal. Mater. 20-21:673-678.

Gu, B., Schmitt, J., Chen, Z., Liang, L., Mccarthy, J.F., 1994. Adsorption and desorption of natural organic matter on iron oxide: mechanisms and models. Environ. Sci. Technol. 28 (1), 38-46.

Ho, Y., 2006. Review of second-order models for adsorption systems. J. Hazard. Mater. 136 (3), 681-689.

Hu, J., Zevi, Y., Kou, X., Xiao, J., Wang, X., Jin, Y., 2010. Effect of dissolved organic matter on the stability of magnetite nanoparticles under different pH and ionic strength conditions. Sci. Total. Environ. 408 (16), 3477-3489.

Illés, E., Tombácz, E., 2006. The effect of humic acid adsorption on pH-dependent surface charging and aggregation of magnetite nanoparticles. J. Colloid Interface Sci. 295 (1), 115-123.

Kondo, S., Ishikawa, T., Abe, I., 2006. Adsorption science. Chemical Industry Press, Beijing.

Kun, Y., Daohui, L., Baoshan, X., 2009. Interactions of humic acid with nanosized inorganic oxides. Langmuir 25 (6), 3571-3576.

Liang, L., Luo, L., Zhang, S., 2011. Adsorption and desorption of humic and fulvic acids on SiO2 particles at nano- and micro-scales. Colloids Surf. A 384 (1–3), 126-130.

Philippe, A., Schaumann, G.E., 2014. Interactions of dissolved organic matter with natural and engineered inorganic colloids: a review. Environ. Sci. Technol. 48 (16), 8946-8962.

Qiu, H., Lv, L., Pan, B., Zhang, Q., Zhang, W., Zhang, Q., 2009. Critical review in adsorption kinetic models. J. Zhejiang U.-SCI. A 10 (5), 716-724.

Speight, J.G., 2005. Lange's handbook of chemistry (sixteenth edition). McGraw-Hill, New York.